Acceptance Angle Influence on the Optimum Incident Spot Size for High-Finesse Microcavity Two-Photon Absorption Photodetectors

John O'Dowd, Wei-Hua Guo, Michael Lynch, A. Louise Bradley, and John F. Donegan, *Senior Member, IEEE*

***Abstract*—The influence of the limited acceptance angle of a high-finesse microcavity two-photon absorption photodetector on its response has been investigated. It is shown that the limited acceptance angle of the microcavity explains the observed asymmetry seen in the spectral dependence of the microcavity. The theory describing the influence of the acceptance angle allows for an optimum incident beam waist for any cavity structure to be calculated, with an optimum spot diameter of 7 μm having been calculated for the microcavity under test. The theory also enables the calculation of an optimum incident spot size for any microcavity. It is shown that a cavity with higher overall reflectivity require larger input spot sizes in order to optimize the level of generated two-photon absorption.**

***Index Terms*—Acceptance angle, photodetector, planar microcavity, two-photon absorption (TPA).**

I. Introduction

TWO-PHOTON absorption (TPA) in semiconductors has recently received interest as it can be employed to characterize very short optical pulses, with characterization of optical pulses as short as 6 fs using TPA in GaAsP having been demonstrated [1]. TPA in silicon has been shown as a means of harvesting electrical energy using the two-photon photovoltaic effect [2]. TPA has been shown to be useful in measuring numerous network impairments such as chromatic dispersion [3], optical signal-to-noise-ratio (OSNR) [4] and polarization mode dispersion [5]. However, TPA in semiconductors is always a very inefficient process. To improve the detection sensitivity various detectors have been proposed, such as waveguide detectors with a very long absorption length [6] and avalanche photodiodes with a very high internal gain [7]. These schemes have achieved great improvement in detection sensitivity; however they still suffer from the residual single-photon absorption (SPA) problem. This residual SPA results in a requirement for high peak input signal powers in order for TPA to be dominant so optical amplifiers are needed in order to use these detectors on low peak power optical pulses such as those found in optical telecommunications systems. Single-photon counters are reported to have a high TPA sensitivity and low residual SPA, but they need complex electric circuits to identify effective counts from dark counts [8].

Using a high-finesse planar microcavity to improve the TPA efficiency is a promising technique. Our group has previously demonstrated that the use of a microcavity can enhance the level of TPA by a factor of $>10{,}000$ when compared with the non cavity case [9]. A microcavity has also been shown to preferentially enhance TPA relative to SPA [10]. To further reduce the requirement for high peak power input signals one simple and convenient technique is to focus the light onto the detector to make the focused spot size as small as possible. As TPA is inversely proportional to the spot area while SPA is independent of spot area a smaller spot size results in an increased TPA signal while the SPA signal remains unchanged. For microcavity detectors, there is a trade off associated with the decreased spot size. A high-finesse microcavity has a limited acceptance angle which is associated with the spectral width of the cavity. A tightly focused spot produces incident components some of which have large incidence angles that exceed the acceptance angle of the cavity. In this paper, we analyze the influence of the limited acceptance angle of high-finesse microcavities on the TPA enhancement achieved by these cavities. We also analyze the dependence of the cavity spectrum on the spot size of the incident signal. This analysis allows for the calculation of an incident spot size for any TPA microcavity detector which allows the level of generated TPA to be optimized.

II. Theoretical Analysis

We consider a continuous wave (CW) Gaussian beam normally incident on a microcavity detector. The enhancement of a short optical pulse in a microcavity has previously been analyzed in [11]. Shown in Fig. 1(a) is a Gaussian beam incident from air onto the microcavity detector surface, with the surface of the detector shown in Fig. 1(b).

The electric field of the Gaussian beam can be expressed in air as

$$e_{in}(x,y,z) = \frac{\mathrm{e}_0}{\sqrt{1+z^2\rho_0^{-2}}} \exp\left(-\frac{x^2+y^2}{w^2(z)}\right) \cdot \exp\left(-i\beta\frac{x^2+y^2}{2H(z)}\right) \quad (1)$$

where $\rho_0 = \pi w_0^2 \lambda^{-1}$, $H(z) = z + \rho_0^2 z^{-1}$, $w(z) = w_0(1 + z^2\rho_0^{-2})^{1/2}$, e_0 is the input amplitude, $\beta = 2\pi/\lambda$

Manuscript received January 13, 2009; revised March 19, 2009. Current version published November 18, 2009. This work was supported by SFI under its CSET Centre for Telecommunications Value-Chain Research (CTVR) Grant 03/CE3/I405, and its RFP Programme under Grant RFP/2006/ENE012.

The authors are with the Semiconductor Photonics Group, School of Physics and CTVR, Dublin 2, Ireland (e-mail: jodowd@tcd.ie; guow@tcd.ie; lynchmi@tcd.ie; bradlel@tcd.ie; jdonegan@tcd.ie).

Color versions of one or more of the figures in this paper are available online at http://ieeexplore.ieee.org.

Digital Object Identifier 10.1109/JQE.2009.2022760

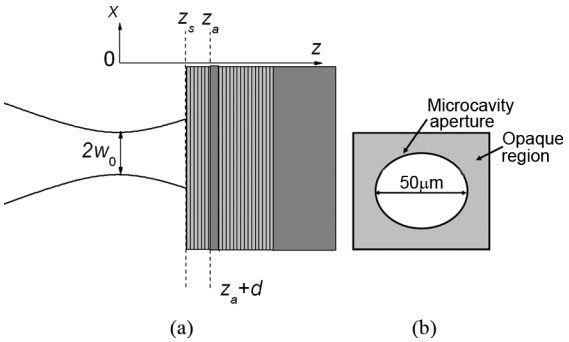

Fig. 1. (a) Schematic diagram of a Gaussian beam normally incident onto a microcavity detector. (b) Schematic of input surface of the detector.

is the wavenumber in vacuum, λ is the incident wavelength, $z = 0$ is the position of the minimum beam waist, x and y are two orthogonal axes which are both orthogonal to z which is the direction of propagation of the Gaussian beam, w_0 is the $1/e$ beam radius at $z = 0$, $w(z)$ is the $1/e$ beam radius at z. To calculate the field in the active layer which is sandwiched between two highly reflective Bragg mirrors, we decompose the field at the detector surface [$z = z_s$ as shown in Fig. 1(a)] into plane waves with different lateral wavenumbers by calculating the Fourier transform

$$\tilde{e}_{\rm in}(k_x, k_y, z_s) = \frac{1}{4\pi^2}\int\int e_{\rm in}(x, y, z_s) \cdot \exp(i(k_x x + k_y y))dxdy \quad (2)$$

where k_x and k_y are the wavenumbers in the x and y directions. Each plane wave component will produce a corresponding wave in the active layer with the change in the incident plane wave characterized by the cavity transfer function

$$\begin{aligned}\Gamma(k_x, k_y, z) &\equiv \frac{\tilde{e}_c(k_x, k_y, z)}{\tilde{e}_{\rm in}(k_x, k_y, z_s)} \\ &= \frac{\sqrt{T_0}\exp(-i\phi_{t_0})}{1 - \sqrt{R_1 R_2}\exp(-i(\phi_{r_1} + \phi_{r_2} + 2k_z d))} \\ &\quad \times\Big(\exp(-ik_z(z - z_a)) + \sqrt{R_2} \\ &\qquad \cdot \exp(-i(2k_z d + \phi_{r_2}))\exp(ik_z(z - z_a))\Big) \quad (3)\end{aligned}$$

where $k_z = (n^2\beta^2 - k_p^2)^{1/2}$, $k_p^2 = k_x^2 + k_y^2$, n is refractive index of the active material, d is the active layer thickness, T_0 is the transmissivity of the front mirror for light incident from air, R_1 and R_2 are front and back mirror reflectivity's for light incident from inside the active region, ϕ_ν (ν represents r_1, r_2 and t_0) are the phase shifts associated with R_1, R_2 and T_0 respectively. The reflection and transmission phase shifts are assumed to be zero for normally incident plane waves at the mode wavelength.

The start position (z_a) of the active layer is shown in Fig. 1(a). The round-trip phase shift $\phi = \phi_{r1} + \phi_{r2} + 2k_z d = 2m\pi$ determines the mode wavelength. If the lateral wavenumbers are equal to zero, i.e., for a normally incident plane wave, the mode wavelength is taken to be λ_0. Around λ_0 the change in the round-trip phase shift ($\Delta\phi$) can be approximated using a first order Taylor expansion as

$$\begin{aligned}\Delta\phi &\equiv \phi(\lambda_0 + \Delta\lambda, k_x, k_y) - \phi(\lambda_0, 0, 0) \\ &= -\frac{4\pi n_g l_\lambda \Delta\lambda}{\lambda_0^2} - \frac{l_\theta k_p^2}{n_0\beta_0} \quad (4)\end{aligned}$$

where

$$l_\lambda = d - \frac{\lambda_0^2}{4\pi n_g}\frac{d\phi_{r_1}}{d\lambda} - \frac{\lambda_0^2}{4\pi n_g}\frac{d\phi_{r_2}}{d\lambda} \quad (5)$$

$$l_\theta = d + n\beta_0\frac{d\phi_{r_1}}{d(k_p^2)} + n\beta_0\frac{d\phi_{r_2}}{d(k_p^2)} \quad (6)$$

where n_0 is the refractive index at λ_0, $\beta_0 = 2\pi/\lambda_0$, l_λ is the effective length of the cavity used in describing the dependence of $\Delta\phi$ on λ, l_θ is the effective length used to describe the dependence of $\Delta\phi$ on incident angle (θ). If $\Delta\phi = 0$, the dependence of the mode wavelength on both the lateral wavenumbers and the incident angle is

$$\Delta\lambda = -\frac{l_\theta\lambda_0}{2n_0 n_g l_\lambda}\sin^2(\theta) \quad (7)$$

where $\sin(\theta) = k_p/\beta_0$, n_g is the group index. In (3) the numerator describes the standing wave distribution and the denominator describes the enhancement achieved by the reflection from the mirrors. As a simplification we assume that the dependence of the transfer function on both the incident wavelength and the lateral wavenumbers is dominated by the change in the denominator, i.e., we neglect the changes in the standing wave distribution with wavelength and the lateral wavenumbers. This simplification is possible for high-finesse microcavities as the deviation of incident wavelength is kept within a few nanometers of λ_0 and the incident angle is less than approximately 50 degrees off normal incidence as angles of incidence within this range have a phase dependence on incidence angle which is linear. The approximated transfer function is

$$\begin{aligned}\Gamma(k_x, k_y) &\approx \frac{f(z)\exp(-i\Delta\phi_{\lambda,t_0})}{1 + \frac{R}{1-R}\left(1 - \exp\left(i\frac{4\pi n_g l_\lambda \Delta\lambda}{\lambda_0^2} + i\frac{l_\theta k_p^2}{n_0\beta_0}\right)\right)} \\ &\quad \cdot \exp\left(i\frac{l_{\theta,t_0}k_p^2}{n_0\beta_0}\right) \quad (8)\end{aligned}$$

where

$$f(z) = \frac{\sqrt{T_0}}{1 - R}\Big(\exp(-in_0\beta_0(z - z_a)) + \sqrt{R_2}\exp(in_0\beta_0(z - z_a))\Big) \quad (9)$$

is the field inside the cavity for a normally incident plane wave at resonance; $\Delta\phi_{\lambda,t_0}$ is the dependence of the phase change in the top mirror on λ for light on its initial transmission through the top mirror (t_0), $R = \sqrt{R_1 R_2}$, l_{θ,t_0} is the dependence of the effective length of the top mirror on θ for t_0. Both $\Delta\phi_{\lambda,t_0}$ and l_{θ,t_0} are calculated from ϕ_{t_0} as in (5) and (6). We then modify (8) using the spectral width and acceptance angle of the cavity as they are both easily measured experimentally. The spectral

width ($\Delta\lambda_{\mathrm{FWHM}}$, full-width at half maximum, FWHM) for normally incident plane waves can be expressed as

$$\Delta\lambda_{\mathrm{FWHM}} = \frac{(1-R)}{\sqrt{R}}\frac{\lambda_0^2}{2\pi n_g l_\lambda}. \tag{10}$$

The cavity acceptance angle with λ_0 incident can be expressed using (7), (10) as

$$\begin{aligned}\Delta\theta_{\mathrm{FWHM}} &= 2\sin^{-1}\left(\sqrt{\frac{(1-R)}{\sqrt{R}}\frac{n_0\lambda_0}{2\pi l_\theta}}\right)\\ &= 2\sin^{-1}\left(\sqrt{\frac{\Delta\lambda_{\mathrm{FWHM}}}{\lambda_0}\frac{n_0 n_g l_\lambda}{l_\theta}}\right).\end{aligned} \tag{11}$$

If λ_0 is incident at an angle half that of the acceptance angle then the intensity inside the cavity will be half the normal incidence value. The cavity spectral width and the acceptance angle are related to each other through (7). We then re-write (8) as (12), shown at the bottom of the page, where $\Delta\beta_{\mathrm{FWHM}} = 2\beta_0\sin(\Delta\theta_{\mathrm{FWHM}}/2)$. With the approximated transfer function we can calculate the field inside the cavity from the inverse Fourier transform. It can also be seen that $\exp(il_{\theta,t_0}k_p^2/n_0\beta_0)\tilde{e}_{in}(kx,ky,z)$ is the Fourier transform of $e_{\mathrm{in}}(x,y,z_s' \equiv z_s + 2l_{\theta,t_0}/n_0)$. The field inside the active layer can now be described as (13), also shown at the bottom of the page, where some unimportant phase factors have been omitted. The field dependence on z is $f(z)$ in (12) and is omitted in (13) for compactness. With (13) we can calculate the electric field in the active layer and the level of TPA. We use a relative value called the correction factor (C) to describe the cavity effect which is defined as the ratio between the TPA generated in the active layer with and without the influence of the cavity's limited acceptance angle.

$$\zeta = \zeta_0\frac{\int\int|e_c(x,y)|^4dxdy}{\int\int|e_{\mathrm{in}}(x,y,z_s')|^4dxdy} \equiv \zeta_0 C \tag{14}$$

where

$$\zeta_0 = \frac{\int_{z_a}^{z_a+d}|f(z)|^4\,dz}{d} = \frac{T_0^2(1+4R_2+R_2^2)}{(1-R)^4} \tag{15}$$

is the TPA enhancement for a normally incident plane wave at resonance. The factor C is a convolution of the dependence of cavity enhancement on both the incident wavelength and incident angle due to changes in $\Delta\phi$ as shown in (4).

III. Investigation of a Microcavity TPA Device

The microcavity used for all simulations and experimental work in this paper is a microcavity which is resonant at 1558.9 nm and has a $1-\lambda$ GaAs active region. The cavity has 14 p-doped $Ga_{0.88}Al_{0.12}As/Ga_{0.1}Al_{0.9}As$ top mirror pairs and 24 n-doped $Ga_{0.1}Al_{0.9}As/Ga_{0.88}Al_{0.12}As$ bottom mirror pairs. The microcavity response is characterized using a signal provided by a continuous wave external cavity tunable laser. The signal is amplified by an Erbium-doped-fiber-amplifier (EDFA) which provides sufficient optical power to access the TPA dominant absorption regime. Due to the generation of TPA photocurrent in a microcavity photodetector being intrinsically polarization sensitive, the signal is passed though a polarization controller so that the polarization onto the detector can be selected [12]. The polarization is rotated so as to maximize the photocurrent at resonance and is then kept constant for these measurements. The polarization controller consists of an input polarizer and a half- and quarter- wave plate. The lens arrangement has been profiled to ensure that the beam it produces has a Gaussian profile with a value of w_0 of $3.5\,\mu$m.

A z-scan measurement was carried out by moving the microcavity along the propagation direction of the input beam. The microcavity is translated from $z = -150\ \mu$m to $z = 150\ \mu$m with the beam remaining centered in the aperture of the microcavity. The input signal for all measurements is placed as close to normally incident on the microcavity as the measurement setup allows. The optimum focus position which is the position which maximizes the TPA response is set as being $z = 0\ \mu$m. From the theory it is found that this z position does not correspond to the z position which has the w_0 centered on the absorbing region.

The optical power on the microcavity was kept constant at 10 mW for the z-scan measurements. As z increases the microcavity is being moved away from the lens. At each z position the spectral dependence of the microcavity with TPA dominant is measured. This spectral response is asymmetric with the TPA response showing stronger wavelength dependence for wavelengths which are greater than λ_0, see Fig. 2. The maximum photocurrent for each focus position is recorded, see Fig. 3. It is

$$\Gamma(k_x,k_y) \approx \exp\left(i\frac{l_{\theta,t_0}k_p^2}{n_0\beta_0}\right)\frac{f(z)\exp\left(-i\Delta\phi_{\lambda,t_0}\right)}{1+\frac{R}{1-R}\left(1-\exp\left(i\frac{1-R}{\sqrt{R}}\frac{2\Delta\lambda}{\Delta\lambda_{\mathrm{FWHM}}}+i\frac{1-R}{\sqrt{R}}\frac{4k_p^2}{\Delta\beta_{\mathrm{FWHM}}^2}\right)\right)} \tag{12}$$

$$\mathrm{e_c(x,y)} \approx \int\int\frac{\mathrm{e}_{in}(\mathrm{x,y,z_s'})\exp(-ik_x x-ik_y y)}{1+\frac{R}{1-R}\left(1-\exp\left(i\frac{1-R}{\sqrt{R}}\frac{2\Delta\lambda}{\Delta\lambda_{\mathrm{FWHM}}}+i\frac{1-R}{\sqrt{R}}\frac{4k_p^2}{\Delta\beta_{\mathrm{FWHM}}^2}\right)\right)}\mathrm{dk}_x\mathrm{dk}_y \tag{13}$$

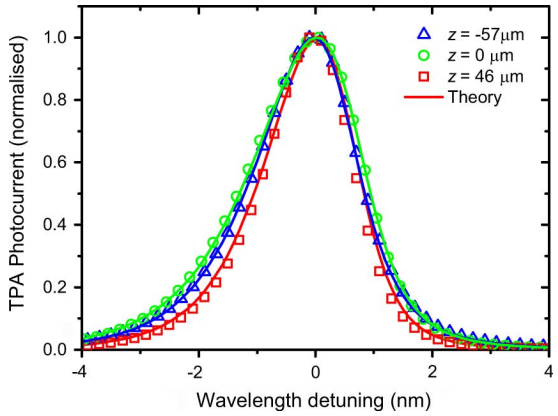

Fig. 2. Wavelength dependence of the microcavity for different focus positions with the microcavity operating in the TPA dominant regime with associated theoretical fits. The wavelength axis of each spectrum is centered and normalized to the maximum TPA response.

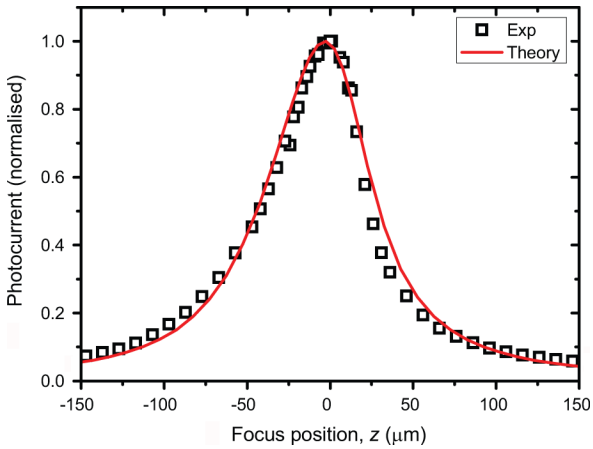

Fig. 3. Dependence of microcavity response on focus position. The focus position axis is centered on the maximum TPA response.

seen that the dependence of the peak TPA response on focus position is asymmetric about $z = 0$ μm. For positions with $z > 0$ μm less TPA is generated than for equivalent distances of $z < 0$ μm. For both Figs. 2 and 3 the contribution of SPA to the detected photocurrent was estimated, as in[10]. It is found for Fig. 2 that while the TPA photocurrent is ≥ 47 nA the SPA photocurrent is approximately 2 nA. When the wavelength is detuned the SPA contribution increases with the TPA photocurrent being > 0.31 nA while the SPA photocurrent is approximately ≥ 0.16 nA. For Fig. 3 the TPA generated photocurrent at $z = 0$ μm is 180 nA while the SPA photocurrent is approximately 1.6 nA. For Fig. 3 at $z = -150$ μm and 150 μm the TPA generated photocurrent is > 10 nA while the SPA photocurrent is approximately 1.6 nA.

In order to fit the observed asymmetry in the microcavity response using the theory outlined above, the spectral width of the microcavity response must be measured. To do this the microcavity is initially placed away from the optimum focus position so that the diameter of the signal incident in the detector is 65 μm. The input signal is larger than the 50 μm in diameter aperture of the microcavity; see Fig. 1(b). With such a

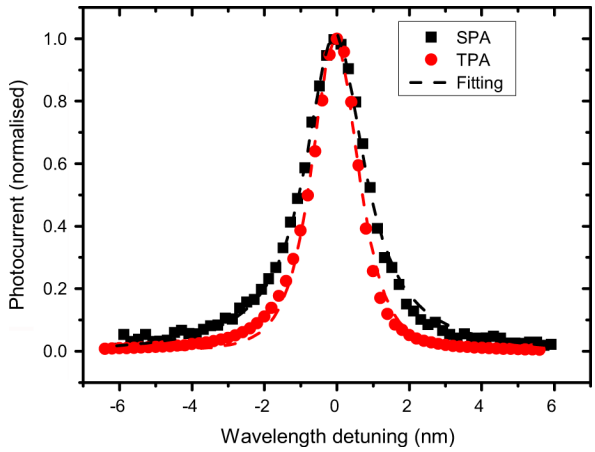

Fig. 4. Wavelength dependence of Microcavity for TPA and SPA dominant regimes with a 65 μm incident spot diameter which corresponds to 30 mW and 1 mW respectively .The dashed lines are the fittings of the SPA and TPA data with a Lorentzian and a Lorentzian squared function respectively.

large spot size it is easier to access the SPA dominant regime. The wavelength is tuned across the cavity resonance for SPA and TPA dominant regimes which are achieved with 1 mW and 30 mW incident on the detector respectively as shown in Fig. 4. The spectral response of the SPA spectrum is fitted using a Lorentzian function. From this fitting $\Delta\lambda_{\mathrm{FWHM}}$ and λ_0 are calculated as being 1.97 nm and 1558.9 nm respectively. The average reflectivity of the microcavity (R) is then calculated using $\Delta\lambda_{\mathrm{FWHM}}/FSR = R^{-1/2}(1-R)/\pi$, which gives a value of R which is 0.963. This corresponds to a cavity finesse of 85.4 and a *FSR* of 168.3 nm. The spectra in Fig. 4 are normalized to the peak photocurrent and their wavelength axis shifted to centre their peak response at the 0 nm position. The remaining two unknowns necessary to fit the microcavity response are l_θ and l_λ. Both l_θ and l_λ are calculated theoretically for the device structure under test using the transverse matrix method, with values of 2.41 μm and 2.04 μm being calculated respectively. The calculated acceptance angle for this cavity is 12.99 degrees.

When fitting the experimental data with the theory, the device is found to be best fit by taking the incident signal on the microcavity as being 4.5 degrees off normal which is within the alignment accuracy of the experimental setup. The angle is included in the theory by adding the momentum resulting from the angle to k_x. The fitting of both the spectral and focus position dependence of the TPA response are shown in Figs. 2 and 3 respectively to fit the experimental data well. The asymmetry in the spectral response in Fig. 2 is due the angular dependence of the cavity resonance wavelength (7). Since the input signal is focused some of the input signal is resonant at wavelengths less than λ_0. The asymmetry in the peak TPA response shown in Fig. 3 is due to the resultant effective spot size of the focused signal in the absorbing region of the microcavity. For $z < 0$ (converging beam) the effective spot size decreases due to multiple roundtrips in the cavity whereas for a diverging beam the effective spot size is larger than the incident spot size. From the theory it is found that the TPA response is not maximized when w_0 is centered in the cavity. The signal is instead maximized approximately 17 μm from this position which corresponds to

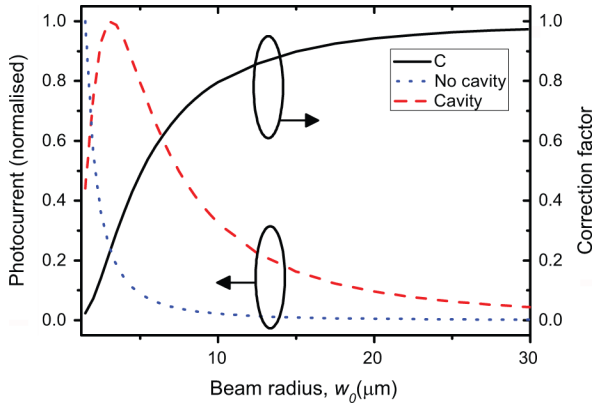

(a)

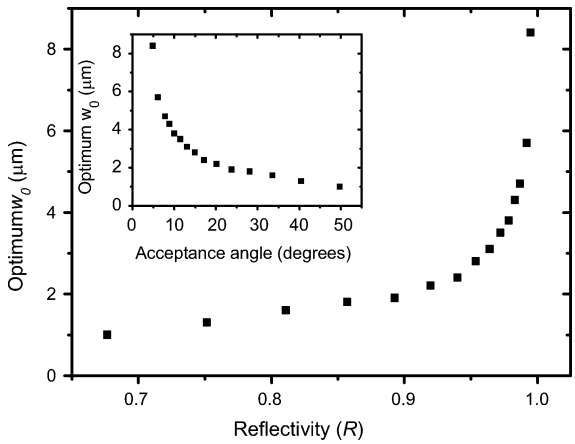

(b)

Fig. 5. (a) Theoretical TPA response versus w_0 of incident beam for non cavity case (dotted line) with the photocurrent normalized to the signal generated by Gaussian signal with $w_0 = 1.5$ μm, cavity case (solid line) is normalized to peak TPA response. Also shown (dashed line) is the response of the correction factor (C) versus w_0. (b) Dependence of optimum input ω_0 on average microcavity reflectivity, (b) (inset) Dependence of optimum input ω_0 on microcavity acceptance angle.

a converging input optical signal being input onto the microcavity.

Using the theory a value of w_0 for the input signal can be calculated which optimizes the level of TPA generated in the microcavity. This is done by simulating the dependence of C on w_0, as described by (14). In the absence of a cavity, the TPA response $(\int\int |e_{\text{in}}(x,y,z_s')|^4 dxdy)$ is inversely proportional to the spot area, see Fig. 5(a). The TPA response in the cavity $(\int\int |e_c(x,y)|^4 dxdy)$ is more complicated. As the value of w_0 is changed so to does the resonant wavelength and the optimum focus position (value of z) of the cavity. In the theoretical analysis, when calculating the level of TPA generated for each value of w_0 the values of λ and z are changed so as to optimize the TPA response. The peak TPA response for each value of w_0 is recorded; see Fig. 5(a). We find that the spot size which maximizes the TPA response in the cavity is not the smallest possible spot size. The value of C is also shown versus w_0. The TPA generated in the cavity relative to the non-cavity case increases with increasing spot size, as the input signal is more efficiently coupled to the resonant cavity mode. The optimum w_0 for the microcavity structure under test was calculated as being 3.5 μm. Once the incident spot size exceeds the optimum value the level of TPA generated in the structure decreases. This is due to the increasing spot area dominating the cavity TPA response. The value of C is shown to approach 1 as the incident spot size becomes larger as the incident beam becomes more like a plane wave. The optimum spot size for an arbitrary microcavity structure is also simulated. The structures simulated all have the same bottom mirror as the microcavity under test but the number of top mirrors is varied in order to find the dependence of the optimum w_0 value on R, see Fig. 5(b). It is shown that for larger values of R (approaching 1.00) the optimum incident spot size increases rapidly.

IV. Conclusion

In order to use a TPA detector at low optical input powers tight focusing of the input beam is essential. A planar microcavity has a limited acceptance angle and so different angular components have different levels of enhancement in the cavity. For a high-finesse microcavity TPA detector, this results in an asymmetrical cavity spectral response and also an asymmetrical response to the focus position. The influence of the acceptance angle on the TPA response of the microcavity means that to optimize the level of TPA generated by a microcavity, the optimal spot size for the microcavity must be calculated. In this paper an optimized incident focused spot diameter of 7 μm has been calculated as being optimal so as to maximize the generated TPA photocurrent for the microcavity under test. While measurements were carried out for a microcavity with a reflectivity of 0.963 we have also calculated the optimal incident focused spot size for cavities with different overall reflectivities. With increasing reflectivity the dependence on incident angle becomes increasingly important and as such the optimal incident spot size increases rapidly.

References

[1] J. K. Ranka, A. L. Gaeta, A. Baltuska, M. S. Pshenichnikov, and D. A. Wiersma, "Autocorrelation measurement of 6-fs pulses based on the two-photon-induced photocurrent in a GaAsP photodiode," *Opt. Lett.*, vol. 22, pp. 1344–1346, 1997.

[2] S. Fathpour, K. K. Tsia, and B. Jalali, "Two-photon photovoltaic effect in silicon," *IEEE J. Quantum Electron.*, vol. 43, pp. 1211–1217, 2007.

[3] K. Bondarczuk, P. J. Maguire, L. P. Barry, J. O'Dowd, W. H. Guo, M. Lynch, A. L. Bradley, J. F. Donegan, and H. Folliot, "Chromatic dispersion monitoring of 80-Gb/s OTDM data signal via two-photon absorption in a semiconductor microcavity," *Photon. Technol. Lett.*, vol. 19, pp. 21–23, Jan. 2007.

[4] M. Dinu, D. C. Kilper, and H. R. Stuart, "Optical performance monitoring using data stream intensity autocorrelation," *J. Lightw. Technol.*, vol. 24, pp. 1194–1202, 2006.

[5] S. Wielandy, M. Fishteyn, and B. Zhu, "Optical performance monitoring using nonlinear detection," *J. Lightw. Technol.*, vol. 22, pp. 784–793, Mar. 2004.

[6] F. R. Laughton, J. H. Marsh, and A. H. Kean, "Very sensitive two-photon absorption GaAs/AlGaAs waveguide detector for an autocorrelator," *Electron. Lett.*, vol. 28, pp. 1663–1665, 1992.

[7] K. Kikuchi, "Highly sensitive interferometric autocorrelator using Si avalanche photodiode as two-photon absorber," *Electron. Lett.*, vol. 34, pp. 123–125, 1998.

[8] C. Xu, J. M. Roth, W. H. Knox, and K. Bergman, "Ultra-sensitive autocorrelation of 1.5 μm light with single photon counting silicon avalanche photodiode," *Electron. Lett.*, vol. 38, pp. 86–88, 2002.

[9] H. Folliot, M. Lynch, A. L. Bradley, L. A. Dunbar, J. Hegarty, J. F. Donegan, L. P. Barry, J. S. Roberts, and G. Hill, "Two-photon absorption photocurrent enhancement in bulk AlGaAs semiconductor microcavities," *Appl. Phys. Lett.*, vol. 80, pp. 1328–1330, Feb. 2002.

[10] W. H. Guo, J. O'Dowd, E. Flood, T. Quinlan, M. Lynch, A. L. Bradley, J. F. Donegan, K. Bondarczuk, P. J. Maguire, and L. P. Barry, "Suppression of residual single-photon absorption relative to two-photon absorption in high finesse planar microcavities," *IEEE Photon. Technol. Lett.*, vol. 20, pp. 1426–1428, 2008.

[11] W. H. Guo, J. O'Dowd, M. Lynch, A. L. Bradley, J. F. Donegan, and L. P. Barry, "Influence of cavity lifetime on high-finesse microcavity two-photon absorption photodetectors," *IEEE Photon. Technol. Lett.*, vol. 19, pp. 432–434, Mar. 2007.

[12] J. O'Dowd, W. H. Guo, E. Flood, M. Lynch, A. L. Bradley, L. P. Barry, and J. F. Donegan, "Polarization dependence of a GaAs-based two-photon absorption microcavity photodetector," *Opt. Expr.*, vol. 16, pp. 17682–17688, 2008.

John O'Dowd was born in Sligo, Ireland, in 1981. He received the B.A.(mod) degree from the School of Physics, Trinity College, Dublin, Ireland, in 2004, where he is currently working toward the Ph.D. degree in physics.

His research interests include two-photon absorption in semiconductor microcavities, and the monitoring of optical networks.

Wei-Hua Guo was born in Hubei Province, China, in 1976. He received the B.Sc. degree in physics from Nanjing University, Nanjing, China, in 1998, and the Ph.D. degree from the Institute of Semiconductors, Chinese Academy of Sciences, Beijing, China, in 2004. His Ph.D. research was on FDTD simulation and fabrication of optical microcavities and design of semiconductor optical amplifiers.

Since September 2004, he has been a Postdoctoral Researcher in the Department of Physics, Trinity College, Dublin, Ireland. His current research is focused on optimizing microcavity two-photon absorption photodetectors based on GaAs material system and designing tunable integrated sources for coherent WDM systems.

Michael Lynch received the B.Sc. degree in applied physics from Dublin City University.

He is a Senior Researcher with the Semiconductor Photonics Group in the School of Physics, Trinity College Dublin. His current research interests are nonlinear optics in semiconductor microcavities and laser diode-based gas sensing.

A. Louise Bradley graduated with a first class Hons. B.Sc. from University College Dublin in 1992. She received the M.Sc. degree in 1994 and the Ph.D., for the study of cavity polaritons using nonlinear optical technique, from Trinity College Dublin in 1998 as part of the European project, SMILES.

She went on to work on the development of GaP microcavity light emitting diodes and later GaN devices under the European project AGETHA. She joined Trinity College in 2001, where she is a Senior Lecturer in the School of Physics. Her current research interests include semiconductor devices for optical communications and novel structures for controlling semiconductor light emission.

Dr. Bradley is a member of the Institute of Physics.

John F. Donegan (M'04–SM'08) received the B.Sc. and Ph.D. degrees in physics from National University of Ireland, Galway, Ireland.

He held postdoctoral positions in Lehigh University, Bethlehem, PA, and the Max Planck Institute, Stuttgart, Germany. He is a Professor of physics with Trinity College, Dublin, Ireland. His research interests are in photonic structures including broadly tunable lasers based on etched slots, microcavity two-photon absorption detectors, spherical microcavity structures, and photonic molecules. He also studies the interaction of quantum dots with human macrophage cells.

Prof. Donegan is a member of the American Physical Society, and a Fellow of the Institute of Physics and the Institute of Nanotechnology.